Frontiers of Information Technology & Electronic Engineering
www.jzus.zju.edu.cn; engineering.cae.cn; www.springerlink.com
ISSN 2095-9184 (print); ISSN 2095-9230 (online)
E-mail: jzus@zju.edu.cn

Physical human-robot interaction estimation based control scheme for a hydraulically actuated exoskeleton designed for power amplification

Yi LONG[1,2], Zhi-jiang DU[1], Wei-dong WANG[1], Long HE[3], Xi-wang MAO[3], Wei DONG[†‡1]

[1]*State Key Laboratory of Robotics and System, Harbin Institute of Technology, Harbin 150001, China*

[2]*Zhongshan Torch Group Co., Ltd., Zhongshan 528400, China*

[3]*Weapon Equipment Research Institute, China South Industries Group Corporation, Beijing 102202, China*

[†]E-mail: dongwei@hit.edu.cn

Received Oct. 26, 2016; Revision accepted Apr. 26, 2017; Crosschecked Sept. 9, 2018

Abstract: We proposed a lower extremity exoskeleton for power amplification that perceives intended human motion via human-exoskeleton interaction signals measured by biomedical or mechanical sensors, and estimates human gait trajectories to implement corresponding actions quickly and accurately. In this study, torque sensors mounted on the exoskeleton links are proposed for obtaining physical human-robot interaction (pHRI) torque information directly. A Kalman smoother is adopted for eliminating noise and smoothing the signal data. Simultaneously, the mapping from the pHRI torque to the human gait trajectory is defined. The mapping is derived from the real-time state of the robotic exoskeleton during movement. The walking phase is identified by the threshold approach using ground reaction force. Based on phase identification, the human gait can be estimated by applying the proposed algorithm, and then the gait is regarded as the reference input for the controller. A proportional-integral-derivative control strategy is constructed to drive the robotic exoskeleton to follow the human gait trajectory. Experiments were performed on a human subject who walked on the floor at a natural speed wearing the robotic exoskeleton. Experimental results show the effectiveness of the proposed strategy.

Key words: Exoskeleton; Physical human-robot interaction; Torque sensor; Human gait; Kalman smoother
https://doi.org/10.1631/FITEE.1601667 **CLC number:** TP242

1 Introduction

Lower limb exoskeletons are intelligent devices that can improve the function of users' limbs and have attracted the interest of many researchers in recent years. Many kinds of lower limb exoskeleton robots are investigated for power amplification, e.g., the Berkeley lower extremity exoskeleton (BLEEX) (Kazerooni et al., 2005; Zoss et al., 2006), a hybrid assistive limb (HAL) (Sankai, 2011), and other robotic rehabilitation systems (Aphiratsakun and Parnichkun, 2010). The general lower limb exoskeleton robot is composed of two mechanical legs, which are parallel to the human limbs. The primary goal of lower extremity exoskeleton control is to perceive the operator's intended motion via a highly cooperative methodology. There are two sources of information to acquire human intended motion, i.e., biomedical signals and physical human-robot interaction (pHRI) force (Lee et al., 2012).

Biomedical information, e.g., eletroencephalogram (EEG), electrooculogram (EOG), and electromyographic (EMG) signals, is collected directly by electrical sensors attached to the human body. EMG, commonly applied in an exoskeleton such as an HAL, is generated by electrical depolarization of muscle during muscular contraction and nerve pulses. The

‡ Corresponding author

collected EMG signals from the surface of muscles can reflect the activation of muscles (Najarian and Splinter, 2012). EMG can predict the body's movement in advance and can be expressed as a function of the strength and the speed of muscle activities (Yin et al., 2012). The HAL system uses EMG signals to estimate the user's intended motion, which builds the mapping between the actuation torque and the filtered EMG signals (Kasaoka and Sankai, 2001; George et al., 2011). However, the relationship between EMG signals and a human's intended motion is highly nonlinear and difficult to obtain directly (Kiguchi and Imada, 2009). The EMG activities of lower limb muscles in normal and pathological gaits can be the guide for a lower limb exoskeleton design (Mishra et al., 2012). This is an effective way to use the EMG to infer a human's intended motion (Fleischer and Hommel, 2008). However, it is inconvenient to use EMG sensors because they must be attached to the user's body and their measurement accuracy is seriously affected by the surface condition of human skin.

A pHRI-based control strategy has been used in some lower limb robots successfully. The force-based interface provides a higher information transmission rate than EMG-based interfaces (Lobo-Prat et al., 2014). The obtained physical interaction force signal is more reliable than a biomedical signal (Lee et al., 2008). To overcome the deficiency mentioned previously, a pHRI-based control strategy has been proposed (Pons, 2008). In essence, the pHRI-based control strategy for exoskeletons renders the pHRI force or torque close to zero, and achieves cooperative human exoskeleton control consequently. The exoskeleton robot WEAR, developed by Sarcos Research, uses force sensors to collect information between the robot and the user to control the exoskeleton's movement (Dollar and Herr, 2008). Another exoskeleton WPS, developed by Kanagawa Institute of Technology, uses muscle hardness sensors to measure the HRI (Yamamoto et al., 2004; Yoshimitsu and Yamamoto, 2004). A wearable exoskeleton robot uses force sensors to acquire the human gait information via the robot's dynamic model (Deng et al., 2007). However, these are typical model-based applications, whose performance depends on the accurate mathematical dynamic modeling of the robotic exoskeleton system.

In this study, a hydraulically actuated lower limb exoskeleton for power amplification is developed. The torque sensors are applied to obtain the pHRI torque directly. A Kalman smoother is used to eliminate signal noise and to smooth the signal for pHRI torque. A predefined relationship between the pHRI torque and the human gait trajectory is designed. A proportional-integral-derivative (PID) control strategy is designed to drive the exoskeleton to follow the human gait trajectory.

2 Exoskeleton hardware configuration

2.1 Mechanical design

Based on ergonomic principles, the exoskeleton design needs to be multi-functional and maintain the comfort of the lower limbs of the human body. The robotic exoskeleton design is shown in Fig. 1. Many design requirements and details are similar to those reported by Long et al. (2016a, 2016b, 2016c, 2017).

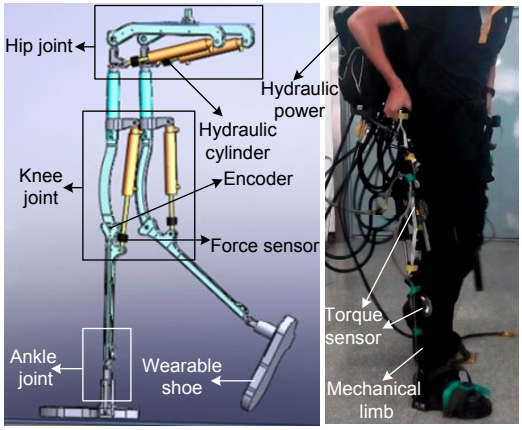

Fig. 1 Prototype of the lower-limb powered exoskeleton
There are two active degrees of freedom for each leg, and all auxiliary facilities are packaged in the backpack

The exoskeleton is composed of two legs with seven degrees of freedom (DOFs) for each leg, which is close to the architecture of human limbs. The flexion/extension of the ankle, knee, and hip needs more power than other DOFs. The flexion/extension of the hip and knee joints is actuated by hydraulic actuators. The ankle is a hinge-type synovial joint, which has three DOFs. When a human user stands, the weight from carrying loads can be transferred to

the ground along the mechanical frame. Passive DOFs of the ankle joint ensure the stability during standing. The actual angular positions of the active joints are measured by optical encoders and the actuation force produced by a hydraulic cylinder is acquired by force sensors.

2.2 Control system

A valve-based hydraulic actuation system is used in the robotic exoskeleton due to its high ratio of power to weight. The hydraulic actuation system includes the following components: double-acting hydraulic cylinders, servo control valves, a direct-current (DC) motor, and a pump. The solenoid serve valve receives control signals from the motion control card and responds with a corresponding movement. The configuration of the control system is shown in Fig. 2. The sensing and communication system consists of three major parts, i.e., torque signal collection, force signal collection (foot pressure and hydraulic cylinder feedback force), and the position feedback with an optical encoder in the control loop. The first part includes four torque sensors, which measure the pHRI torque and transfer it to a data acquisition card through a controller area network (CAN) bus, and to the PC through a USB eventually. The second part includes six foot-pressure sensors and four force sensors, which measure the foot reaction force on the vertical dimension and detect dynamic action of the hydraulic cylinders, respectively. The data are acquired by a 14-channel A/D card and transferred to the PC through a USB. The third part includes the closed-loop position control, in which four encoders are used to actuate four joints respectively. The motion control card transfers the information from the encoders back to the PC through an Ethernet connection.

Safety precautions in the form of hardware and software design are considered for users wearing the system. In the hardware design, some mechanical stoppers are used to insure that the movement of joints is restricted to the appropriate zone, and cannot exceed the natural movement of human joints. External emergency shutoff switches are used to terminate the motor command signal and turn off the power. In the software control design, the safety threshold is designed to protect the human user.

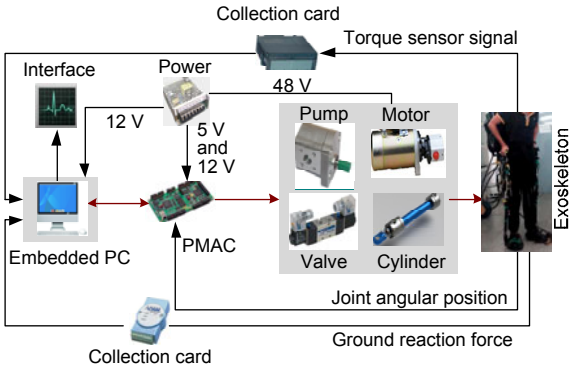

Fig. 2 Architecture of the control system, consisting of signal collection, motion control, and actuation part
All hardware parts are placed together in the control enclosure

3 Intention-driven exoskeleton control

3.1 Human gait trajectory acquisition

3.1.1 Mapping from the pHRI torque to the gait trajectory of the human limb

In this study, a human gait is defined as the trajectory of active joints. The HRI between the human limbs and the exoskeleton can be collected by mechanical sensors, e.g., force sensors and torque sensors. The primary goal of measuring the HRI signal is to obtain information about intended motion. In this study, a one-dimensional torque sensor is used to measure the HRI torque. The torque sensor is fixed at the connection cuff on the thigh or the calf of a single leg. There are two torque sensors for each mechanical leg, one of which is for the knee joint and the other for the hip joint (Fig. 3). The torque sensors are placed on the mechanical legs to detect the pHRI torque.

The torque sensor on the thigh is used for movement detection of the hydraulic actuation system of the hip joint, while the other sensor on the shank for the hydraulic actuator of the knee joint. The signals collected by these two torque sensors are recorded as $T_H(k)$ and $T_K(k)$ at the k^{th} interval for the hip joint and the knee joint, respectively. In fact, the output of the torque sensor is directional. The angular positions of the hip joint and the knee joint are defined as $\theta_H(k)$ and $\theta_K(k)$ respectively, and the increments of $\theta_H(k)$ and $\theta_K(k)$ are defined as $\Delta\theta_H(k)$ and $\Delta\theta_K(k)$ respectively. The human gait can be represented as $\boldsymbol{\theta}(k)=[\theta_H(k), \theta_K(k)]^T$, which can be

expressed as follows:

$$\begin{cases}\theta_{\mathrm{H}}(k)=\theta_{\mathrm{H}}(k-1)+\Delta\theta_{\mathrm{H}}(k),\\ \theta_{\mathrm{K}}(k)=\theta_{\mathrm{K}}(k-1)+\Delta\theta_{\mathrm{K}}(k),\end{cases} \tag{1}$$

where $\theta_{\mathrm{H}}(0)=0$ and $\theta_{\mathrm{K}}(0)=0$ are the initial values of the hip joint and the knee joint, respectively.

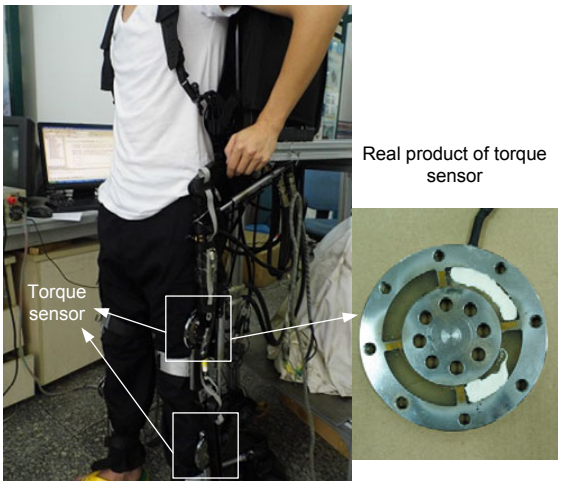

Fig. 3 Diagram of torque sensor placements on the lower limb

The primary goal of the human gait acquisition is to find the mappings from $T_{\mathrm{H}}(k)$ to $\Delta\theta_{\mathrm{H}}(k)$, and $T_{\mathrm{K}}(k)$ to $\Delta\theta_{\mathrm{K}}(k)$. The mapping should have two features: (1) the HRI $\Delta\boldsymbol{\theta}(k)=[\Delta\theta_{\mathrm{H}}(k),\ \Delta\theta_{\mathrm{K}}(k)]^{\mathrm{T}}$ has a significant positive correlation with $\boldsymbol{T}(k)=[T_{\mathrm{H}}(k),\ T_{\mathrm{K}}(k)]^{\mathrm{T}}$; (2) $\Delta\boldsymbol{\theta}(k)$ is saturated when $\boldsymbol{T}(k)$ is large enough. The mapping can be expressed as follows:

$$\begin{cases}\Delta\boldsymbol{\theta}(k)=\boldsymbol{A}(k)\times\boldsymbol{T}(k),\\ \boldsymbol{A}(k)=\mathrm{diag}\{a_1(k),a_2(k)\},\ a_1(k)>0,\ a_2(k)>0,\end{cases} \tag{2}$$

where $a_1(k)$ and $a_2(k)$ are two positive constants tuned in real applications. This kind of mapping is depicted in Fig. 4, where $T_{\mathrm{c}}(k)$ is the critical point for the HRI, $a_i(k)=\tan\beta$ (i=1, 2), and $\Delta\theta_{\mathrm{max,P}}(k)$ and $\Delta\theta_{\mathrm{max,N}}(k)$ are the maximum values in the positive and negative directions, respectively. When $T_{\mathrm{c}}(k)$ occurs, the human user will feel extremely uncomfortable.

Actually, the values of $\boldsymbol{A}(k)$ have a significant effect on the velocity of human limbs. They are determined by the rate of change in the pHRI torque $\boldsymbol{T}(k)$, expressed as the follows:

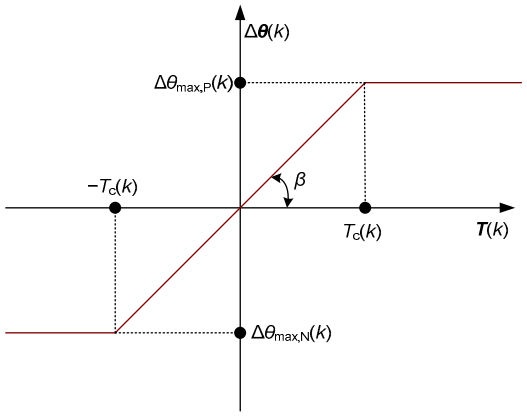

Fig. 4 Mapping from $\boldsymbol{T}(k)$ to $\Delta\boldsymbol{\theta}(k)$

$$\boldsymbol{A}(k)=\boldsymbol{C}\times\Delta\boldsymbol{T}(k), \tag{3}$$

where $\boldsymbol{C}\in\mathbb{R}^{2\times2}$ and $\Delta\boldsymbol{T}(k)\in\mathbb{R}^{2\times2}$,

$$\begin{cases}\boldsymbol{C}=\mathrm{diag}\{c_1,c_2\},\ c_1>0,\ c_2>0,\\ \Delta\boldsymbol{T}(k)=\mathrm{diag}\{T_{\mathrm{H}}(k)-T_{\mathrm{H}}(k-1),\ T_{\mathrm{K}}(k)-T_{\mathrm{K}}(k-1)\}.\end{cases} \tag{4}$$

As discussed previously, the mapping from the HRI to the human gait can be obtained as follows:

$$\boldsymbol{\theta}(k)=\boldsymbol{\theta}(k-1)+\boldsymbol{C}\times\Delta\boldsymbol{T}(k)\times\boldsymbol{T}(k). \tag{5}$$

3.1.2 pHRI torque acquisition and processing

The human gait can be obtained by the collected pHRI torque (Eq. (5)). Generally, the measured pHRI torque includes noises at higher frequencies. The pHRI torque should be processed by a low-pass filter to eliminate noise before it is used in Eq. (5). Compared with the biomedical signal, the measured pHRI torque lags behind the real intended human motion. The delay in pHRI will cause the exoskeleton system to lag behind the human limb movement. In this study, a Kalman smoother is used to deal with the delay. The general state-space representation of a linear time-variant system is given as follows (Welch and Bishop, 2001; Chen, 2012):

$$\begin{cases}\boldsymbol{x}_k=\boldsymbol{A}\boldsymbol{x}_{k-1}+\boldsymbol{B}\boldsymbol{u}_{k-1}+\boldsymbol{Q}_{k-1},\\ \boldsymbol{y}_k=\boldsymbol{H}\boldsymbol{x}_k+\boldsymbol{R}_k,\end{cases} \tag{6}$$

where $\boldsymbol{x}_k$, $\boldsymbol{y}_k$, and $\boldsymbol{R}_k$ are the k^{th} system state, measured output value, and the measurement noise vector respectively, $\boldsymbol{u}_{k-1}$ and $\boldsymbol{Q}_{k-1}$ are the $(k-1)^{\text{th}}$ input to the system and system state noise vector respectively, and $\boldsymbol{A}$, $\boldsymbol{B}$, and $\boldsymbol{H}$ are the state matrix, input matrix, and output matrix respectively. The primary goal of the Kalman filter is to minimize the gap between the predicted value and the actual target value by the least squares method. The updated equations are shown as follows:

$$\begin{cases} \hat{\boldsymbol{x}}_k^- = \boldsymbol{A}\hat{\boldsymbol{x}}_{k-1} + \boldsymbol{B}\boldsymbol{u}_{k-1}, \\ \boldsymbol{P}_k^- = \boldsymbol{A}\boldsymbol{P}_{k-1}\boldsymbol{A}^{\mathrm{T}} + \boldsymbol{Q}_{k-1}, \\ \boldsymbol{K}_k = \boldsymbol{P}_k^-\boldsymbol{H}^{\mathrm{T}}(\boldsymbol{H}\boldsymbol{P}_k^-\boldsymbol{H}^{\mathrm{T}} + \boldsymbol{R}_k), \\ \hat{\boldsymbol{x}}_k = \hat{\boldsymbol{x}}_k^- + \boldsymbol{K}_k(\boldsymbol{y}_k - \boldsymbol{H}\hat{\boldsymbol{x}}_{k-1}), \\ \boldsymbol{P}_k = (\boldsymbol{I} - \boldsymbol{K}_k\boldsymbol{H})\boldsymbol{P}_k^-, \end{cases} \tag{7}$$

where $\boldsymbol{K}_k$ is the Kalman gain matrix, $\boldsymbol{I}$ is the unit matrix, and $\boldsymbol{P}_k$ is the variance matrix. The Kalman filter focuses only on the measurement data before and at time step k. The Kalman smoother is used for all the measurements in the current period. Compared with the Kalman filter, a Kalman smoother can deal with the whole measurement process better.

The Kalman smoother can smooth the signal while eliminating noise. The smoothed distributions over the measurement can be calculated from the Kalman filtering results by recursions as follows (Sarkka et al., 2004):

$$\begin{cases} \boldsymbol{P}_k^- = \boldsymbol{A}\boldsymbol{P}_{k-1}\boldsymbol{A}^{\mathrm{T}} + \boldsymbol{Q}_{k-1}, \\ \boldsymbol{C}_{k-1} = \boldsymbol{P}_{k-1}\boldsymbol{A}_{k-1}^{\mathrm{T}}(\boldsymbol{P}_k^-)^{-1}, \\ \boldsymbol{x}_{k-1}^{\mathrm{s}} = \boldsymbol{x}_{k-1} + \boldsymbol{C}_{k-1}(\boldsymbol{x}_k^{\mathrm{s}} - \boldsymbol{A}\boldsymbol{x}_{k-1}), \\ \boldsymbol{P}_k^{\mathrm{s}} = \boldsymbol{P}_k + \boldsymbol{C}_k(\boldsymbol{P}_k^{\mathrm{s}} - \boldsymbol{P}_k^-)\boldsymbol{C}_{k-1}^{\mathrm{T}}, \end{cases} \tag{8}$$

where $\boldsymbol{x}_{k-1}^{\mathrm{s}}$ is the $(k-1)^{\text{th}}$ state value via the Kalman smoother, and $\boldsymbol{C}_{k-1}$ is a gain matrix. In this study, Eq. (6) is the system equation for the torque sensor. Those parameters can be defined as

$$\begin{aligned} &\boldsymbol{I} = \begin{bmatrix} 1 & 0 \\ 0 & 0 \end{bmatrix},\ \boldsymbol{A} = \begin{bmatrix} 0 & 1 \\ 1 & 0 \end{bmatrix},\ \boldsymbol{H} = \begin{bmatrix} 1 & 0 \end{bmatrix},\ R = 3, \\ &\boldsymbol{Q} = \begin{bmatrix} 0.1 & 0 \\ 0 & 0.1 \end{bmatrix}, \end{aligned} \tag{9}$$

where the measurement noise R is only a number since the Kalman filter deals with the only one sensor signal. The original pHRI torque is taken from the lower extremity exoskeleton. The curve with high-speed kurtosis can be smoothed by the Kalman smoother. The pHRI torque smooth processing is helpful in achieving a smooth gait trajectory.

3.2 Control strategy design

As mentioned above, the estimated human gait trajectory using pHRI signals is regarded as the reference input for the exoskeleton robot. The control strategy depends on identifying the walking phases. In fact, the walking phases can be identified by the ground reaction force (GRF) to determine which joints of the legs should be actuated. In this study, three force sensors placed in the wearable shoes are used to identify the walking phases, i.e., the stance phase and the swing phase (Long et al., 2015). A simple threshold method is used to distinguish the following four kinds of walking phases: double stance, left stance and right swing, left swing and right stance, and double swing. When the wearer stands upright, the values for GRF can be recorded as $F_{\mathrm{L},1}(0)$, $F_{\mathrm{L},2}(0)$, $F_{\mathrm{L},3}(0)$, $F_{\mathrm{R},1}(0)$, $F_{\mathrm{R},2}(0)$, and $F_{\mathrm{R},3}(0)$ for the left leg and right leg, respectively. Define the sum of GRF values for a single leg as follows:

$$\begin{cases} F_{\mathrm{L,A}}(0) = F_{\mathrm{L},1}(0) + F_{\mathrm{L},2}(0) + F_{\mathrm{L},3}(0), \\ F_{\mathrm{R,A}}(0) = F_{\mathrm{R},1}(0) + F_{\mathrm{R},2}(0) + F_{\mathrm{R},3}(0), \end{cases} \tag{10}$$

where $F_{\mathrm{L,A}}(0)$ and $F_{\mathrm{R,A}}(0)$ are the initial sum of GRF in the double stance. Those four walking phases can be obtained according to the initial sum of values and the real time GRF values. Define

$$\begin{cases} F_{\mathrm{L,A}}(k) = F_{\mathrm{L},1}(k) + F_{\mathrm{L},2}(k) + F_{\mathrm{L},3}(k), \\ F_{\mathrm{R,A}}(k) = F_{\mathrm{R},1}(k) + F_{\mathrm{R},2}(k) + F_{\mathrm{R},3}(k), \end{cases} \tag{11}$$

where $F_{\mathrm{L,A}}(k)$ and $F_{\mathrm{R,A}}(k)$ are the sum of values in the k^{th} interval. The walking phases can be obtained according to Algorithm 1. Note that the walking phase is regarded as the triggering condition for human gait tracking. To avoid chattering, each judgment condition will be doubled to make sure it is stable. Three kinds of walking phases are identified, i.e., double stance, left stance and right swing, and left swing and

right stance. This kind of phase identification method is valid and effective in the preliminary stage of robotic exoskeleton development. In the future work, the gait phase identification will be optimized to obtain maximum accuracy and consistency.

Algorithm 1 Walking phases based on the threshold method

Initialization: Collect the GRF values 2000 times when the operator stands up straight

for i=1, 2, ..., 2000 **do**
  $F_{L,A}(i)=F_{L,1}(i)+F_{L,2}(i)+F_{L,3}(i)$
  $F_{R,A}(i)=F_{R,1}(i)+F_{R,2}(i)+F_{R,3}(i)$
end for
Obtain the sum of the GRF values at the initial state $F_{L,A}(0)=F_{L,A}/2000$, $F_{R,A}(0)=F_{R,A}/2000$
Initialize weight parameters α_L, β_L, α_R, and β_R to satisfy $\alpha_L<1<\beta_L$ and $\alpha_R<1<\beta_R$
Collect GRF values $F_{L,A}(k)=F_{L,1}(k)+F_{L,2}(k)+F_{L,3}(k)$ and $F_{R,A}(k)=F_{R,1}(k)+F_{R,2}(k)+F_{R,3}(k)$
if $\alpha_L F_{L,A}(0)\le F_{L,A}(k)\le\beta_L F_{L,A}(0)$ **or** $F_{L,A}(k)>\beta_L F_{L,A}(0)$ **and** $\alpha_R F_{R,A}(0)\le F_{R,A}(k)\le\beta_R F_{R,A}(0)$ **or** $F_{R,A}(k)>\beta_R F_{R,A}(0)$
  Output P=1 (double stance)
else
  if $F_{L,A}(k)>\beta_L F_{L,A}(0)$ **or** $\alpha_L F_{L,A}(0)\le F_{L,A}(k)\le\beta_L F_{L,A}(0)$ **and** $F_{R,A}(k)<\alpha_R F_{R,A}(0)$
    Output P=2 (left stance and right swing)
  else
    if $F_{L,A}(k)<\alpha_L F_{L,A}(0)$ **and** $F_{R,A}(k)>\beta_R F_{R,A}(0)$ **or** $\alpha_R F_{R,A}(0)\le F_{R,A}(k)\le\beta_R F_{R,A}(0)$
      Output P=3 (left swing and right stance)
    end if
  end if
end if

The trajectory of the active joints can be obtained by Algorithm 2, where $\theta_{H,L}(k)$, $\theta_{K,L}(k)$, $\theta_{H,R}(k)$, and $\theta_{K,R}(k)$ are angular positions of the left hip joint, left knee joint, right hip joint, and right knee joint respectively, $T_{H,L}(k)$, $T_{K,L}(k)$, $T_{H,R}(k)$, and $T_{K,R}(k)$ are torque signals for the left hip joint, left knee joint, right hip joint, and right knee joint respectively. The stance phase is mainly for transferring the load to the ground surface while the swing phase for tracking the human gait trajectory. The controller is to actuate the exoskeleton robot to follow and assist compliantly the human legs to reduce the pressure imposed on the human body. The control process for the exoskeleton can be divided into two steps: acquiring the human gait trajectory using the measured torque signal, and controlling the exoskeleton to track the reference trajectory.

Algorithm 2 Phase identification-based human gait acquisition

Initialization: Current phase, P={1, 2, 3, 4}, C=diag{$C_{H,L}$, $C_{K,L}$, $C_{H,R}$, $C_{K,R}$}

if P=1
  $\theta_{H,L}(k)=\theta_{H,L}(k-1)$, $\theta_{K,L}(k)=\theta_{K,L}(k-1)$, $\theta_{H,R}(k)=\theta_{H,R}(k-1)$, $\theta_{K,R}(k)=\theta_{K,R}(k-1)$
  The knee joint and the hip joint keep its current position, respectively
else
  if P=2
    $\theta_{H,L}(k)=\theta_{H,L}(k-1)+C_{H,L}\Delta T_{H,L}(k)T_{H,L}(k)$
    $\theta_{K,L}(k)=\theta_{K,L}(k-1)$, the left knee keeps the current position
    $\theta_{H,R}(k)=\theta_{H,R}(k-1)+C_{H,R}\Delta T_{H,R}(k)T_{H,R}(k)$
    $\theta_{K,R}(k)=\theta_{K,R}(k-1)+C_{K,R}\Delta T_{K,R}(k)T_{K,R}(k)$
  else
    if P=3
      $\theta_{H,R}(k)=\theta_{H,R}(k-1)+C_{H,R}\Delta T_{H,R}(k)T_{H,R}(k)$
      $\theta_{K,R}(k)=\theta_{K,R}(k-1)$, the right knee keeps the current position
      $\theta_{H,L}(k)=\theta_{H,L}(k-1)+C_{H,L}\Delta T_{H,L}(k)T_{H,L}(k)$
      $\theta_{K,L}(k)=\theta_{K,L}(k-1)+C_{K,L}\Delta T_{K,L}(k)T_{K,L}(k)$
    end if
  end if
end if

The block diagram for the whole control strategy is shown in Fig. 5. The collected pHRI torque data are processed by the Kalman smoother (Eqs. (6) and (8)). The processed pHRI torque data are used to estimate the human gait using Eq. (5). The estimated human gait will be sent to the execution part to drive the mechanical legs to move along with the human limbs. The actual joint angular positions are collected in real time by the optical encoders. A general PID control algorithm is adopted to actuate the exoskeleton to shadow the estimated human joint trajectory. The protocol for the control software is shown in Fig. 6. The modularized control software structure includes four parts: data acquisition module, control module, execution module, and robotic exoskeleton. The data acquisition module is used to collect four kinds of sensor signals: GRF, pHRI, angular position of the

joint, and hydraulic actuation force. The control module is used to acquire the human gait trajectory based on the proposed algorithm. The execution module includes a programmable multi-axis controller (PMAC) and a hydraulic actuation system. The execution module drives the robotic exoskeleton to follow the estimated human gait.

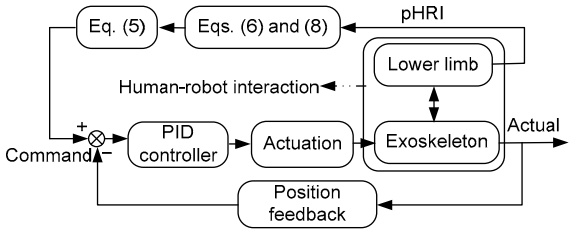

Fig. 5 Control diagram for the exoskeleton
The outside loop obtains the joint trajectory from the torque signal; the inner loop is to control the exoskeleton to follow the joint trajectory

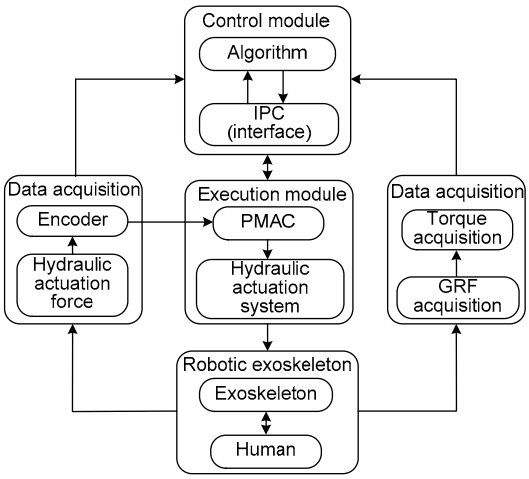

Fig. 6 Modularized structure of the control software

4 Case study: walking wearing exoskeleton

4.1 Experimental platform

In this subsection, the proposed method was examined through experiments on level ground (Fig. 7). The auxiliary facilities in the backpack include the hydraulic actuator system, the control enclosure, and the power supply. To verify the proposed method, laboratory experiments were performed on a healthy subject. The human subject was required to stand up straight when wearing the exoskeleton and start the system when she/he wants to move forward. Before using the robotic exoskeleton system, the whole system should be checked to make sure that all electrical equipment, all sensors, and the hydraulic actuation system are working normally. The user weared the exoskeleton and standed up straight to conduct a self-check of the system. A healthy subject weared the exoskeleton to walk on the floor at a natural speed of about 0.8 m/s and the maximum velocity can be up to 4 km/h with 30 kg loads.

4.2 Analysis of results

As Fig. 7 shows, the experiment was performed on level ground. The torque sensors on the thigh and shank were used to acquire the pHRI torque between the wearer and the exoskeleton. Based on the obtained pHRI torque, the human gait trajectory can be estimated by Eq. (5). The PID controller gave the command signals to the hydraulic actuators to drive the robotic exoskeleton to follow the acquired human gait trajectory. To illustrate the effectiveness of the proposed method, different kinds of data were collected in real time during the experiments, i.e., GRF signals for gait phase identification, pHRI signals to estimate the human gait trajectory, encoder signals for feedback from the angular position of the actual joints,

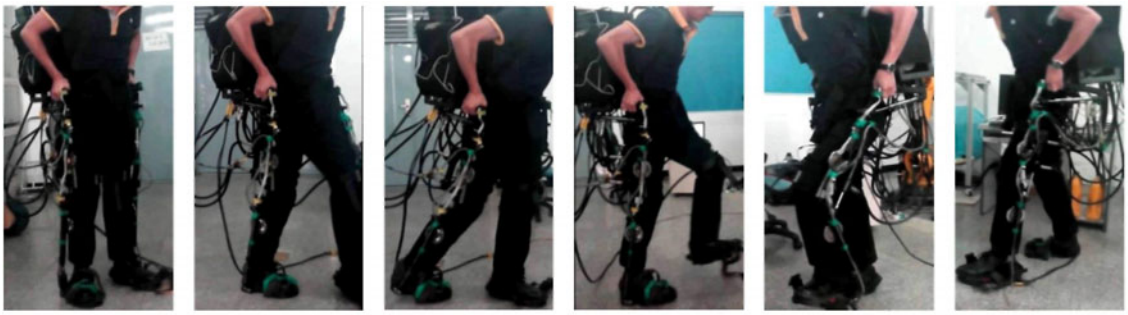

Fig. 7 Human subject walking on level ground in the experiment

and force sensor signals to obtain hydraulic cylinder actuation information.

Based on the proposed method, the mappings from the pHRI signals to the human gait trajectory for the knee joint and the hip joint are illustrated in Figs. 8 and 9, respectively. 'HRI' in the legend means the signals collected from the torque sensor, 'Gait' means the acquired human gait trajectory, and 'Reference' is a zero-value line. In Fig. 8, the pHRI value is positive between points *A* and *B*, during which the human gait trajectory between points *D* and *E* increases continuously. The pHRI value is negative between points *B* and *C*, which causes the human gait trajectory to decrease along the negative direction, as seen in the curve from points *E* to *F*. Figs. 8 and 9 show that the pHRI determines both the amplitude and the direction of the human gait. The pHRI changes in the (−2, 2) N·m interval, while the acquired human gait is located at (−20, 75) deg. The human gait trajectory tracking is demonstrated in Figs. 10 and 11. Figs. 10 and 11 denote the trajectory trackings for the knee joint and hip joint, respectively. Note that in Fig. 10, the negative angular position of the human gait is forced to zero in the high-level controller since the mechanical legs cannot extend beyond a straight state in the stance phase. The collected human gait trajectory of the knee joint is continuous, where the negative angular position is not valid in the low-level controller. Overall, the mechanical legs can track the estimated human gait trajectory. In the future work, improvements in tracking performance will be studied to enhance the wearing comfort.

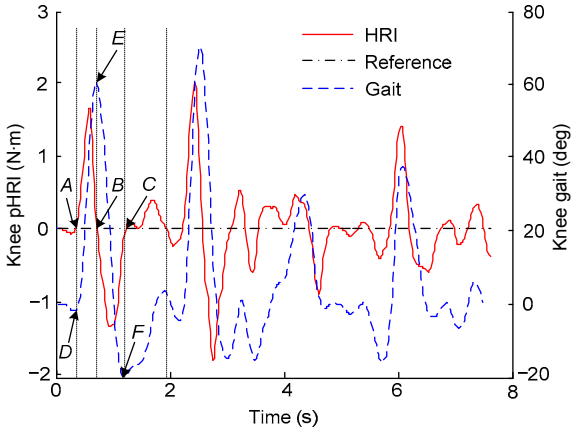

Fig. 8 Relationship between the pHRI torque and the knee joint in a human subject

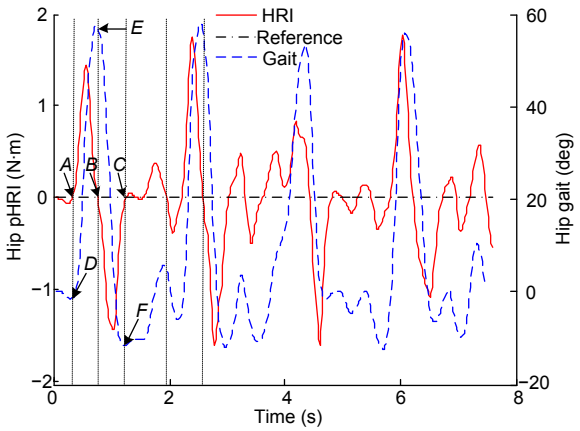

Fig. 9 Relationship between the pHRI torque and the hip joint in a human gait

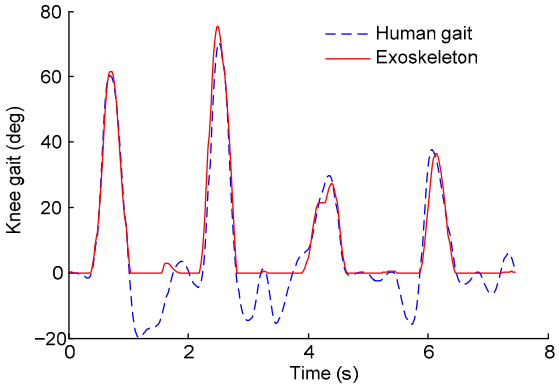

Fig. 10 Human gait trajectory in tracking the knee joint

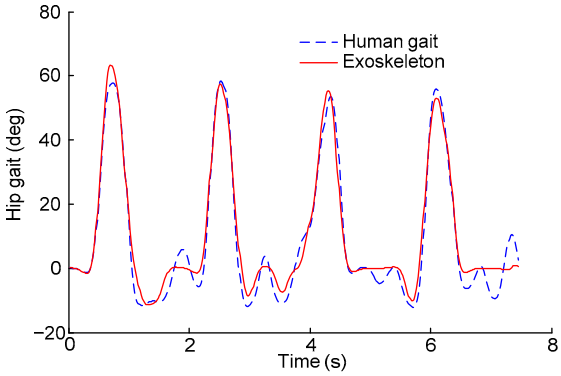

Fig. 11 Human gait trajectory in tracking the hip joint

5 Conclusions

In this study, a robotic exoskeleton system actuated by a hydraulic system for motion assistance and load carrying has been studied. A one-dimensional

torque sensor has been used to measure the HRI between the wearer and the exoskeleton in the sagittal plane. The mapping from the HRI to the human gait has been defined according to a real application. A simple identification algorithm for the walking phase has been proposed to construct the state machine for the control scheme. This work provides an alternative method for developing a lower extremity exoskeleton for power amplification. Experiments have been performed with a human subject wearing the exoskeleton. The experimental results showed that the proposed method is effective and valid, and can be extended and employed in similar assistive exoskeletons. Therefore, other adaptive robust controllers should be studied in the future for actuating an exoskeleton robot to follow human movement without delay and synchronize with the wearer accurately, e.g., adaptive PID control, sliding mode control, and intelligent control.

References

Aphiratsakun N, Parnichkun M, 2010. Balancing control of leg exoskeleton using ZMP-based Jacobian compensation. *Int J Rob Autom*, 25(4):359-371. https://doi.org/10.2316/Journal.206.2010.4.206-3434

Chen SY, 2012. Kalman filter for robot vision: a survey. *IEEE Trans Ind Electron*, 59(11):4409-4420. https://doi.org/10.1109/TIE.2011.2162714

Deng XH, Shen HH, Chen F, et al., 2007. Motion information acquisition from human lower limbs for wearable robot. Int Conf on Information Acquisition, p.137-142. https://doi.org/10.1109/ICIA.2007.4295713

Dollar AM, Herr H, 2008. Lower extremity exoskeletons and active orthoses: challenges and state-of-the-art. *IEEE Trans Rob*, 24(1):144-158. https://doi.org/10.1109/TRO.2008.915453

Fleischer C, Hommel G, 2008. A human-exoskeleton interface utilizing electromyography. *IEEE Trans Rob*, 24(4):872-882. https://doi.org/10.1109/TRO.2008.926860

George T, Shalu GK, Sivanandan KS, 2011. Sensing, processing and application of EMG signals for HAL (hybrid assistive limb). Int Conf on Sustainable Energy and Intelligent Systems, p.749-753. https://doi.org/10.1049/cp.2011.0463

Kasaoka K, Sankai Y, 2001. Predictive control estimating operator's intention for stepping-up motion by exoskeleton type power assist system HAL. IEEE/RSJ Int Conf on Intelligent Robots and Systems, p.1578-1583. https://doi.org/10.1109/IROS.2001.977204

Kazerooni H, Racine JL, Huang L, 2005. On the control of the Berkeley lower extremity exoskeleton (BLEEX). IEEE Int Conf on Robotics and Automation, p.4353-4360. https://doi.org/10.1109/ROBOT.2005.1570790

Kiguchi K, Imada Y, 2009. EMG-based control for lower-limb power-assist exoskeletons. IEEE Workshop on Robotic Intelligence in Informationally Structured Space, p.19-24. https://doi.org/10.1109/RIISS.2009.4937901

Lee H, Kim W, Han J, 2012. The technical trend of the exoskeleton robot system for human power assistance. *Int J Prec Eng Manuf*, 13(8):1491-1497. https://doi.org/10.1007/s12541-012-0197-x

Lee HD, Yu SN, Lee SH, et al., 2008. Development of human-robot interfacing method for assistive wearable robot of the human upper extremities. Int Conf on Instrumentation, Control and Information Technology (SICE Annual Conf), p.1755-1760. https://doi.org/10.1109/SICE.2008.4654948

Lobo-Prat J, Keemink AQL, Stienen AHA, et al., 2014. Evaluation of EMG, force and joystick as control interfaces for active arm supports. *J Neuroeng Rehabil*, 11(1):68. https://doi.org/10.1186/1743-0003-11-68

Long Y, Du ZJ, Wang WD, 2015. A fuzzy logic system tuned with particle swarm optimization for gait segmentation using insole measured ground reaction force. World Congress on Intelligent Control and Automation, p.513-518. https://doi.org/10.1109/WCICA.2014.7052766

Long Y, Du ZJ, Wang WD, et al., 2016a. Development of a wearable exoskeleton rehabilitation system based on hybrid control mode. *Int J Adv Rob Syst*, 13(5):1-10. https://doi.org/10.1177/1729881416664847

Long Y, Du ZJ, Wang WD, et al., 2016b. PSO-SVM-based online locomotion mode identification for rehabilitation robotic exoskeletons. *Sensors*, 16(9):1408. https://doi.org/10.3390/s16091408

Long Y, Du ZJ, Wang WD, et al., 2016c. Robust sliding mode control based on GA optimization and CMAC compensation for lower limb exoskeleton. *Appl Bion Biomech*, 2016:5017381. https://doi.org/10.1155/2016/5017381

Long Y, Du ZJ, Dong W, et al., 2017. Human gait trajectory learning using online Gaussian process for assistive lower limb exoskeleton. In: Yang CJ, Virk GS, Yang HY (Eds.), Wearable Sensors and Robots. Springer, Singapore, p.165-179. https://doi.org/10.1007/978-981-10-2404-7_14

Mishra AK, Srivastava A, Tewari RP, et al., 2012. EMG analysis of lower limb muscles for developing robotic exoskeleton orthotic device. *Proc Eng*, 41:32-36. https://doi.org/10.1016/j.proeng.2012.07.139

Najarian K, Splinter R, 2012. Biomedical Signal and Image Processing. CRC Press, Boca Raton, USA.

Pons JL, 2008. Wearable Robots: Biomechatronic Exoskeletons. John Wiley & Sons, Hoboken, USA, p.127-163.

Sankai Y, 2011. HAL: hybrid assistive limb based on cybernics. In: Kaneko M, Nakamura Y (Eds.), Robotics Research. Springer Berlin Heidelberg, p.25-34. https://doi.org/10.1007/978-3-642-14743-2_3

Sarkka S, Vehtari A, Lampinen J, 2004. Time series prediction by Kalman smoother with cross-validated noise density.

IEEE Int Joint Conf on Neural Networks, p.1653-1657. https://doi.org/10.1109/IJCNN.2004.1380209

Welch G, Bishop G, 2001. An Introduction to the Kalman Filter. Technical Report, University of North Carolina, Chapel Hill, USA, p.1-16.

Yamamoto K, Ishii M, Noborisaka H, et al., 2004. Standalone wearable power assisting suit-sensing and control systems. IEEE Int Workshop on Robot and Human Interactive Communication, p.661-666. https://doi.org/10.1109/ROMAN.2004.1374841

Yin YH, Fan YJ, Xu LD, 2012. EMG and EPP-integrated human-machine interface between the paralyzed and rehabilitation exoskeleton. *IEEE Trans Inform Technol Biomed*, 16(4):542-549. https://doi.org/10.1109/TITB.2011.2178034

Yoshimitsu T, Yamamoto K, 2004. Development of a power assist suit for nursing work. SICE Annual Conf, p.577-580.

Zoss AB, Kazerooni H, Chu A, 2006. Biomechanical design of the Berkeley lower extremity exoskeleton (BLEEX). *IEEE/ASME Trans Mechatron*, 11(2):128-138. https://doi.org/10.1109/TMECH.2006.871087